

Cite this article

de Araújo JM (2019)

A non-linear model for analysis and design of slender reinforced-concrete columns.

Magazine of Concrete Research 71(6): 287–297,<https://doi.org/10.1680/jmacr.17.00428>**Research Article****Paper 1700428**

Received 16/09/2017; Revised 26/12/2017;

Accepted 09/01/2018;

Published online 05/03/2018

Keywords: finite element methods/
structural analysis/structural design

ICE Publishing: All rights reserved

A non-linear model for analysis and design of slender reinforced-concrete columns

José Milton de Araújo DEng

Professor, Engineering School, Federal University of Rio Grande,

Rio Grande, RS, Brazil (ed.dunas@mikrus.com.br)

(Orcid:0000-0002-8459-6985)

The purpose of this paper is to present a non-linear model for analysis and design of slender reinforced-concrete columns subjected to uniaxial and biaxial bending. This model considers both material and geometric non-linearities, as well as creep effects. The structural analysis is performed by the finite-element method associated with an iterative process to solve the system of non-linear equations. The column may have an arbitrary polygonal cross-section, including openings. Green's theorem is used to perform the integration at the level of the cross-sections, which is greatly simplified with the use of a new parabola–rectangle diagram proposed for concrete in compression. This new diagram provides the correct value of the tangent modulus of elasticity of concrete, allowing its use for non-linear analysis of slender columns. By changing the strain value corresponding to the maximum stress, it is possible to use a single stress–strain diagram for displacement calculation and rupture verification, which facilitates the design of slender columns. The accuracy of the method is demonstrated through the analysis of several columns tested experimentally by other authors.

Notation

A_{cc}	compressed area in column cross-section	m	number of reinforcement bars in cross-section
A_s	total area of reinforcement in column cross-section	N	axial force
A_{si}	area of each bar of reinforcement	n	exponent of parabola–rectangle diagram
b	width of rectangular cross-section	p	percentage of stress reduction after stress peak in concrete
E_{cd}	design modulus of elasticity of concrete	R	ratio between theoretical failure load and experimental failure load
E_{cm}	tangent modulus of elasticity of concrete	R_m	mean value of R
$E_{c,par}$	modulus of elasticity obtained with parabola–rectangle diagram	t	height of a rectangular cross-section
E_s	modulus of elasticity of reinforcement	u_o	axial displacement in the z -direction
e_x	eccentricity of axial force in the x -direction	V_R	coefficient of variation of R
e_y	eccentricity of axial force in the y -direction	W	transverse displacement
e_1	first-order eccentricity	W_x	transverse displacement in the x -direction
F_d	design axial load	W_y	transverse displacement in the y -direction
F_g	sustained load	(x_{si}, y_{si})	coordinates of generic reinforcement bar
F_u	failure load	γ_c	partial safety factor for concrete
$F_{u,exp}$	experimental failure load	γ_{cE}	partial safety factor for modulus of elasticity of concrete
$F_{u,p}$	theoretical rupture load, considering $p\%$ of post-peak-stress reduction	γ_s	partial safety factor for reinforcement
$F_{u,teo}$	theoretical failure load	ϵ_c	compressive strain of concrete
$F_{u,0}$	theoretical rupture load, considering $p = 0$	ϵ_{co}	modified strain corresponding to the maximum stress in concrete
f_{cd}	design compressive strength of concrete	ϵ_{c2}	strain corresponding to maximum stress in concrete
f_{ck}	characteristic compressive strength of concrete	ϵ_{cu2}	rupture strain of concrete
f_{cm}	mean compressive strength of concrete	ϵ_o	axial strain
f_y	mean yield strength of reinforcement	ϵ_s	strain of reinforcement
f_{yd}	design yield strength of reinforcement	ϵ_y	yield strain of reinforcement
f_{yk}	characteristic yield strength of reinforcement	ϵ_z	normal strain
h	height of cross-section	ζ	ageing coefficient
L	length of column	λ	slenderness ratio
M	bending moment	λ_x	slenderness ratio in the x -direction
M_x	bending moment in the x -direction (around the y -axis)	λ_y	slenderness ratio in the y -direction
M_y	bending moment in the y -direction (around the x -axis)	σ_c	concrete compressive stress
		σ_R	standard deviation of R

σ_s	steel stress
σ_{si}	stress in each bar of reinforcement
ϕ	creep ratio
ϕ_{ef}	effective creep ratio
χ_x	curvature in the plane $z-x$
χ_y	curvature in the plane $z-y$

Introduction

In the design of slender reinforced-concrete columns, it is necessary to consider material and geometric non-linearities. The material non-linearity is due to the non-linear behaviour of the concrete and of the reinforcement after the yielding. The geometric non-linearity arises from the need to verify the equilibrium in the deformed structure. Bending moments in the initial undeformed configuration of the column axis are called first-order moments. The additional moments caused by deformations are called second-order moments. Owing to the importance of this element for structural stability, design codes, such as CEB-FIP Model Code 1990 (CEB, 1990), Eurocode 2 (BSI, 2004), fib Model Code 2010 (fib, 2010) and ACI 318-14 (ACI, 2014), require that the additional second-order effects be considered in the design of columns. Only in very short columns is it allowed to ignore the second-order moments (Narayanan and Beeby, 2005).

For columns with small or medium slenderness, design codes allow the use of simplified methods to consider second-order and creep effects in the design of concrete columns. Eurocode 2 (BSI, 2004), for example, adopts two simplified methods for second-order analysis of slender reinforced-concrete columns: a method based on nominal stiffness and a method based on nominal curvature. The first method is similar to the moment magnification procedure adopted by ACI 318-14 (ACI, 2014). The second method is also recommended by CEB-FIP Model Code 1990 (CEB, 1990) and by fib Model Code 2010 (fib, 2010). These simplified methods have been extensively studied in order to improve their accuracy (Barros *et al.*, 2010; Bonet *et al.*, 2007, 2011).

When the column is very slender and the second-order effects are very important, it is necessary to perform a complete non-linear analysis, where non-linearities are considered appropriately. This analysis requires the use of numerical methods, such as the finite-element method or the finite-difference method, associated with iterative and incremental techniques for solving the system of non-linear equations (Bouchaboub and Samai, 2013; Kwak and Kim, 2004; Lou *et al.*, 2015; Pires and Silva, 2014).

The objective of this paper is to present a non-linear model for analysis and design of slender reinforced-concrete columns subjected to uniaxial and biaxial bending. This model considers both material and geometric non-linearities, as well as creep effects. The structural analysis is performed using the

finite-element method. The Broyden–Fletcher–Goldfarb–Shanno (BFGS) iterative method is used to solve the system of non-linear equations. Columns may have an arbitrary polygonal cross-section, including openings. Green's theorem is used to perform the integrations required to determine the sectional forces. A new parabola–rectangle diagram for compressed concrete is also proposed in this paper. The accuracy of the method is demonstrated through the analysis of several columns tested experimentally by other authors. As a continuation of this paper, the non-linear model can be used to verify the simplified methods presented in the design codes.

Constitutive models for materials

When comparing the theoretical model with experimental results, the mean yield strength of reinforcement f_y and the mean compressive strength of concrete f_{cm} should be considered. The concrete in tension is neglected in the analysis even if uncracked.

Figure 1 shows the stress–strain diagram adopted for reinforcing steel. The value of the modulus of elasticity E_s is assumed equal to 200 GPa. This diagram is employed for tension and compression, limiting the tensile strain to 10‰ as a failure criterion. For concrete in compression the parabola–rectangle diagram shown in Figure 1 is adopted. The stress and strain are represented by their absolute values.

According to Eurocode 2 (BSI, 2004), the strains ε_{c2} and ε_{cu2} are given by

- $\varepsilon_{c2}(\text{‰}) = 2.0, \quad \text{if } f_{ck} \leq 50 \text{ MPa}$
- $\varepsilon_{c2}(\text{‰}) = 2.0 + 0.085 (f_{ck} - 50)^{0.53}, \quad \text{if } f_{ck} > 50 \text{ MPa}$
- $\varepsilon_{cu2}(\text{‰}) = 3.5, \quad \text{if } f_{ck} \leq 50 \text{ MPa}$

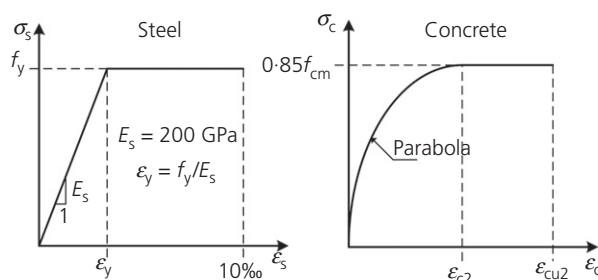


Figure 1. Stress–strain diagrams for materials

Offprint provided courtesy of www.icevirtuallibrary.com
Author copy for personal use, not for distribution

$$4. \quad \varepsilon_{cu2}(\%) = 2.6 + 35 \left(\frac{90 - f_{ck}}{100} \right)^4, \quad \text{if } f_{ck} > 50 \text{ MPa}$$

In these equations, f_{ck} is the characteristic compressive cylinder strength of concrete in MPa. The equation of the parabola is given by

$$5. \quad \sigma_c = 0.85f_{cm} \left[1 - \left(1 - \frac{\varepsilon_c}{\varepsilon_{c2}} \right)^n \right], \quad \text{for } 0 \leq \varepsilon_c \leq \varepsilon_{c2}$$

where $0.85f_{cm}$ is the maximum stress that occurs when $\varepsilon_c = \varepsilon_{c2}$.

According to Eurocode 2 (BSI, 2004), the exponent n is given by

$$6. \quad n = 2, \quad \text{if } f_{ck} \leq 50 \text{ MPa}$$

$$7. \quad n = 1.4 + 23.4 \left(\frac{90 - f_{ck}}{100} \right)^4, \quad \text{if } f_{ck} > 50 \text{ MPa}$$

The parabola–rectangle diagram, with these definitions for the exponent n , is only recommended for the design of cross-sections. It should not be used for non-linear analysis because the derivative $d\sigma_c/d\varepsilon_c$ does not provide a coherent value for the modulus of elasticity, particularly for concrete with $f_{ck} > 50$ MPa. Using Equation 5 and taking the derivative $d\sigma_c/d\varepsilon_c$ when $\varepsilon_c = 0$, one can obtain the tangent modulus of elasticity $E_{c,par} = 0.85n f_{cm}/\varepsilon_{c2}$ provided by the parabola–rectangle diagram.

The tangent modulus of elasticity for normal weight concrete can be estimated by

$$8. \quad E_{cm} = 22 \left(\frac{f_{cm}}{10} \right)^{0.3} : \text{GPa}$$

where $f_{cm} = f_{ck} + 8$ MPa is the mean compressive strength of concrete, as recommended by Eurocode 2.

Figure 2 shows the variations of $E_{c,par}$ and E_{cm} as a function of the characteristic compressive strength of concrete f_{ck} .

As shown in Figure 2, the parabola–rectangle diagram gives incorrect values for the modulus of elasticity of concrete. For this reason, this diagram should not be used for non-linear analysis. Eurocode 2 presents a stress–strain relation for non-linear structural analysis, but it is too complex to perform explicit integrations through Green’s theorem.

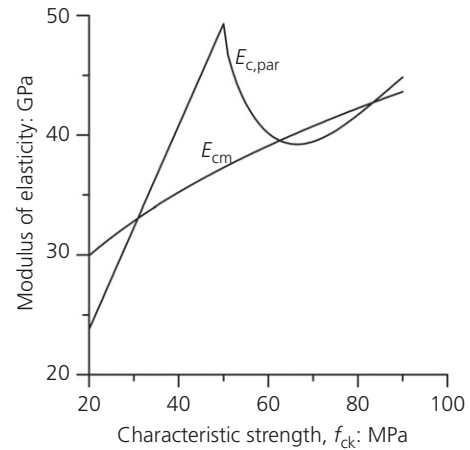


Figure 2. Modulus of elasticity as a function of concrete compressive strength

To correct this problem of the parabola–rectangle diagram, it is proposed that

$$9. \quad n = \frac{E_{cm} \varepsilon_{c2}}{0.85f_{cm}}$$

be the value of the exponent n to be used in Equation 5.

With this new definition of n , we obtain the tangent modulus of elasticity $E_{c,par} = E_{cm}$ at the origin of the stress–strain diagram. This modified parabola–rectangle diagram can be used for non-linear analysis, unlike the original parabola–rectangle diagram of Eurocode 2 (BSI, 2004). It has the advantage of being simpler than the stress–strain relation for non-linear structural analysis adopted by Eurocode 2. The use of the new parabola–rectangle diagram facilitates the integrations necessary to obtain the sectional forces through Green’s theorem.

Figure 3 shows the stress–strain curves obtained with the new parabola–rectangle diagram for several concrete strength classes. To include creep effects, the strains ε_{c2} and ε_{cu2} must be multiplied by $(1 + \phi_{ef})$, where ϕ_{ef} is the effective creep ratio. The effective modulus of elasticity is given by $E_{c,par} = E_{cm}/(1 + \phi_{ef})$.

The curves of Figure 3 do not show a descending part after the maximum stress, as is experimentally observed. This descending part of the stress–strain curve depends strongly on the specimen or member geometry, the boundary conditions and the possibilities for load redistribution in the structure. The descending portion of the stress–strain relation is size dependent and therefore not only a material property (fib, 2010). Previous numerical tests have shown that the rupture loads obtained with the present model do not depend much on the

Offprint provided courtesy of www.icevirtuallibrary.com
Author copy for personal use, not for distribution

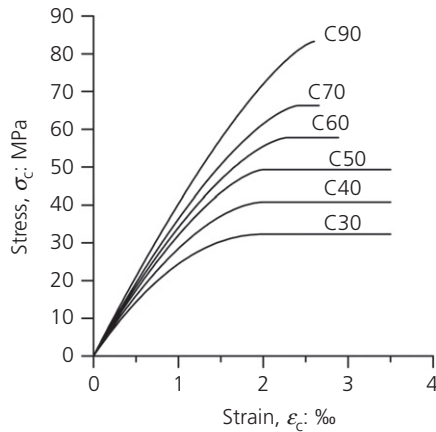


Figure 3. Adopted stress–strain diagrams for concrete

descending portion of the stress–strain diagram. Thus, to simplify the analysis, it is considered that the stress is constant after the strain ϵ_{c2} , as shown in Figure 3. Moreover, the consideration of a constant stress after the strain ϵ_{c2} allows the use of a single stress–strain diagram for the dimensioning of slender columns, as shown in the section ‘Considerations for the design of slender columns’.

Figure 4 shows the ratio between the theoretical rupture load $F_{u,p}$ considering $p\%$ of stress reduction and the theoretical rupture load $F_{u,0}$ considering that the stress is constant after the strain ϵ_{c2} . This figure was obtained for a column of square cross-section under uniaxial bending with different slenderness ratios λ . As can be seen, the descending portion of the stress–strain diagram of concrete only influences the rupture load for very short columns and when considering a very large percentage p . However, even in these cases, the reduction in the rupture load is small.

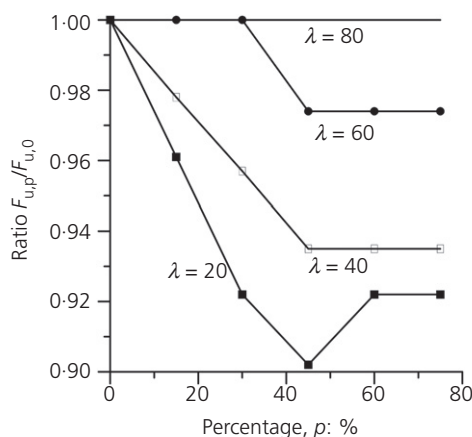


Figure 4. Influence of descending portion of concrete diagram on rupture load

Finite-element analysis

Figure 5 shows a column subjected to the design axial load F_d applied at its ends. The column may have an arbitrary polygonal cross-section, including internal openings. Owing to the shape of the cross-section and the arbitrary point of application of the load, the column is subjected to biaxial bending. In a generic cross-section, the eccentricities of the axial force are e_x and e_y . These eccentricities may vary along the column axis, depending on the first-order moment diagram.

The structural analysis is performed using the finite-element method, where the column axis is discretised in linear elements of two nodes, with five degrees of freedom per node. Each node has a displacement in the z -direction, a displacement in the x -direction, a displacement in the y -direction, a bending rotation around the x -axis and a bending rotation around the y -axis. The torsion of the element is neglected. The stiffness matrix of the element is symmetric and has ten rows and ten columns. The stiffness matrix and the vector of nodal non-linear actions are obtained by numerical integration of Gauss–Legendre, using three integration points along the element axis (Zienkiewicz and Taylor, 2000).

A point located on the element axis undergoes an axial displacement $u_o(z)$ and transverse displacements $W_x(z)$ and $W_y(z)$ in the directions z , x and y , respectively. These displacements are interpolated from the nodal displacements using standard interpolation functions (Araújo, 2014). For the axial displacement, a linear interpolation is used; for the transverse displacements, cubic polynomials are adopted. Employing the well-known strain–displacement relations, the normal strain ϵ_z at coordinates (x, y, z) is given as

$$10. \quad \epsilon_z = \epsilon_o + y\chi_y + x\chi_x$$

where $\epsilon_o = \epsilon_o(z)$ is the axial strain, $\chi_y = -\partial^2 W_y / \partial z^2$ and $\chi_x = -\partial^2 W_x / \partial z^2$ are the curvatures in the z – y and z – x planes, respectively.

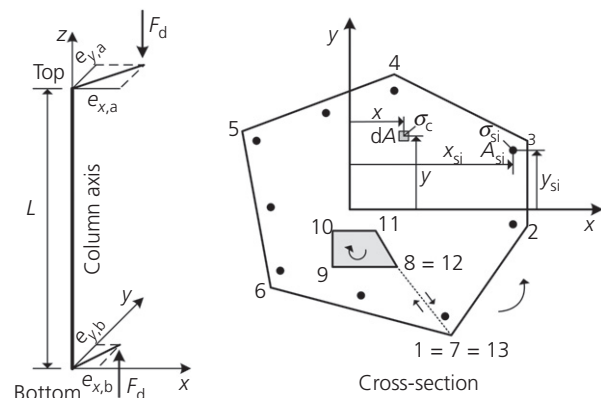


Figure 5. Loading and cross-section of column

Offprint provided courtesy of www.icevirtuallibrary.com
Author copy for personal use, not for distribution

The axial strain is given by

$$11. \quad \varepsilon_o = \frac{\partial u_o}{\partial z} + \frac{1}{2} \left[\left(\frac{\partial W_y}{\partial z} \right)^2 + \left(\frac{\partial W_x}{\partial z} \right)^2 \right]$$

where the last term introduces the geometric non-linearity of the problem.

In this formulation, a positive sign indicates tensile strain and a negative sign indicates compressive strain.

Figure 5 shows the rule for numbering the vertices of the polygonal cross-section. The vertices of the outer contour are numbered counterclockwise. If the section is hollow, the inner contour is numbered clockwise. The last vertex must be coincident with the first vertex to close the polygon.

The cross-section has m reinforcement bars. A generic bar has an area equal to A_{si} and coordinates (x_{si}, y_{si}) . Using Equation 10, one can calculate the strain in each steel bar. The stress σ_{si} in each bar is obtained by employing the stress-strain diagram for reinforcing steel. Similarly, one can calculate the concrete stress σ_c at any point of the cross-section. Applying the equilibrium equations, the following sectional forces are obtained in a cross-section located at the coordinate z along the column axis

$$12. \quad N = \int_{A_{cc}} \sigma_c dA + \sum_{i=1}^m \sigma_{si} A_{si}$$

$$13. \quad M_x = \int_{A_{cc}} \sigma_c x dA + \sum_{i=1}^m \sigma_{si} A_{si} x_{si}$$

$$14. \quad M_y = \int_{A_{cc}} \sigma_c y dA + \sum_{i=1}^m \sigma_{si} A_{si} y_{si}$$

where N is the axial force, M_x is the bending moment in the x direction (around the y axis) and M_y is the bending moment in the y direction (around the x axis).

It should be noted that the integrations are carried out only in the compressed area A_{cc} , because the concrete tensile strength is neglected in the column design. In several studies (Barros *et al.*, 2010; Bouchaboub and Samai, 2013; Kwak and Kim, 2004; Lou *et al.*, 2015), these integrals are solved by discretising the column cross-section into small area elements or layers. This procedure, besides requiring great computational effort, presents difficulty in accurately representing the arbitrary polygonal geometry of the cross-section. By employing rectangular area elements, for example, a very refined discretisation is

required so that the geometry of the polygonal cross-section can be well represented.

Bonet *et al.* (2004) present two alternative methods to solve this problem. The integrations are evaluated using a Gauss quadrature. However, both methods decompose the integration area into thick layers parallel to the most tensile stressed fibre, whose definition depends on the constitutive equation of the concrete.

These drawbacks can be avoided using Green's theorem, as detailed in Araújo (2014). In this solution, the area integrals are replaced by line integrals. This semi-analytical integration requires little computational effort and allows one to accurately represent the geometry of the polygonal cross-section. The sectional forces N , M_x and M_y are used to obtain the non-linear nodal actions, which are derived from the application of the principle of virtual work.

To perform the integrations given in Equations 12 to 14, the compressed area is divided into two regions. Using Equation 10, one obtains the equations of the lines $\varepsilon_z = 0$ (neutral axis) and $\varepsilon_z = \varepsilon_{c2}$. By determining the intersections of these two lines with the sides of the cross-section, the parabola and rectangle regions shown in Figure 6 can be defined. In the polygon named 'parabola', the compressive stress in concrete is given by Equation 5 with n obtained from Equation 9. In the polygon named 'rectangle', we have $\sigma_c = 0.85f_{cm}$. Using Green's theorem, the integrals on the two regions are replaced by line integrals along the sides of these two polygons.

The structural analysis is carried out through an iterative and incremental process. In a given iteration, there will be an imbalance between the vector of non-linear nodal actions and the vector of nodal loads applied on the column. The BFGS method is used to cancel the imbalance and find the deformed configuration of the column for a given loading. Then the loads are increased and the iterative process is again employed.

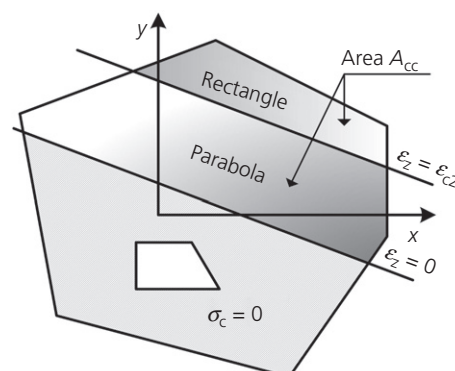


Figure 6. Subdivision of cross-section for use of Green's theorem

Offprint provided courtesy of www.icevirtuallibrary.com
Author copy for personal use, not for distribution

This procedure is repeated successively until the occurrence of failure on an integration point of the finite element, or until the displacements begin to diverge. Failure is assumed when the strain in a reinforcement bar reaches the value 10‰. The failure can also occur by concrete crushing, when the compressive strain at a vertex of the polygonal cross-section reaches ϵ_{cu2} . If the cross-section is fully compressed, the failure is verified on a fibre located at a distance $(1 - \epsilon_{c2}/\epsilon_{cu2})h$ from the most compressed vertex, where h is the height of the cross-section measured perpendicular to the neutral axis. If the strain in this fibre reaches ϵ_{c2} , the occurrence of concrete crushing is considered.

Comparison with experimental results

The model was used to analyse 124 columns tested by other authors, with 20 columns subjected to sustained loads and 104 columns subjected to short-term loads. Tests include 95 columns subjected to uniaxial bending and 29 columns subjected to biaxial bending. The pin-ended columns were subjected to an axial load with constant eccentricities along the axis. The theoretical failure load $F_{u,teo}$ is compared with the experimental failure load $F_{u,exp}$ obtained in the tests.

Previous tests have indicated that the size of the element has little influence on the results. Since the load is applied in constant increments, the model does not capture the post-peak softening response. Thus, all columns were discretised in ten elements and the load was applied in 50 equal increments, obtaining satisfactory accuracy.

Columns tested by Goyal and Jackson

Goyal and Jackson (1971) tested columns subjected to uniaxial bending, with 26 columns under short-term load and 20 columns under sustained load. The slenderness ratio λ ranges from 55 to 125. The columns have square cross-section.

The columns under long-term load were subjected to a sustained load F_g for a period of 6 months. After this period, the load was increased until failure of the column for the load F_u . The creep coefficient measured in the test specimens was $\phi = 2.4$. The effective creep ratio is given by $\phi_{ef} = \zeta \phi F_g / F_u$, where $\zeta = 0.8$ is the ageing coefficient.

Tables 1 and 2 present the results obtained for the columns tested by Goyal and Jackson. For columns subjected to short-term loads, the mean value of the ratio $R = F_{u,teo} / F_{u,exp}$ is

Table 1. Columns subjected to short-term loads tested by Goyal and Jackson (1971)

Column	f_{cm} : MPa	e_i : cm	$F_{u,exp}$: kN	$F_{u,teo}$: kN	$F_{u,teo}/F_{u,exp}$
$L = 182$ cm; $\lambda = 83$; $f_y = 352$ MPa; $A_s = 1.42$ cm ²					
A1	19.9	3.81	33.1	33.1	1.00
A2	19.9	3.81	33.4	33.1	0.99
C1	23.3	2.54	44.5	46.3	1.04
C2	23.3	2.54	46.8	46.3	0.99
E1	21.9	1.27	66.7	64.7	0.97
E2	21.9	1.27	65.4	64.7	0.99
G1	22.2	1.91	55.4	53.2	0.96
G2	22.2	1.91	53.0	53.2	1.00
$L = 182$ cm; $\lambda = 83$; $f_y = 310$ MPa; $A_s = 1.00$ cm ²					
I1	22.7	1.27	60.0	57.6	0.96
I2	22.7	1.27	57.4	57.6	1.00
K1	22.8	1.91	46.6	45.2	0.97
K2	22.8	1.91	45.6	45.2	0.99
M1	22.9	2.54	37.1	37.1	1.00
M2	22.9	2.54	37.0	37.1	1.00
$L = 122$ cm; $\lambda = 55$; $f_y = 310$ MPa; $A_s = 1.00$ cm ²					
O1	23.6	1.27	82.3	79.0	0.96
O2	23.6	1.27	92.4	79.0	0.85
P1	23.6	1.91	64.5	61.9	0.96
P2	23.6	1.91	72.7	61.9	0.85
Q1	19.9	2.54	51.4	46.8	0.91
Q2	19.9	2.54	48.9	46.8	0.96
$L = 274$ cm; $\lambda = 125$; $f_y = 310$ MPa; $A_s = 1.00$ cm ²					
R1	21.4	1.27	33.5	33.5	1.00
R2	21.4	1.27	31.1	33.5	1.08
S1	20.9	1.91	23.0	25.5	1.11
S2	20.9	1.91	24.3	25.5	1.05
T1	20.7	2.54	19.4	21.9	1.13
T2	20.7	2.54	20.6	21.9	1.06

Offprint provided courtesy of www.icevirtuallibrary.com
Author copy for personal use, not for distribution

Table 2. Columns subjected to sustained loads tested by Goyal and Jackson (1971)

Column	f_{cm} : MPa	e_1 : cm	ϕ_{ef}	$F_{u,exp}$: kN	$F_{u,teo}$: kN	$F_{u,teo}/F_{u,exp}$
$L = 182 \text{ cm}; \lambda = 83; f_y = 352 \text{ MPa}; A_s = 1.42 \text{ cm}^2$						
A	19.9	3.81	1.2	32.0	31.4	0.98
B	19.9	3.81	0.8	32.3	32.3	1.00
C	23.3	2.54	1.2	42.9	41.6	0.97
D	23.3	2.54	0.8	40.4	43.2	1.07
E	21.9	1.27	1.3	59.4	55.8	0.94
F	21.9	1.27	0.9	59.3	58.1	0.98
G	22.2	1.91	1.3	50.1	46.6	0.93
H	22.2	1.91	0.9	49.8	48.3	0.97
$L = 182 \text{ cm}; \lambda = 83; f_y = 310 \text{ MPa}; A_s = 1.00 \text{ cm}^2$						
I	22.7	1.27	1.6	44.3	44.3	1.00
J	22.7	1.27	0.8	58.2	50.0	0.86
K	22.8	1.91	1.3	40.9	38.0	0.93
L	22.8	1.91	0.8	43.8	40.3	0.92
M	22.9	2.54	1.2	36.4	32.8	0.90
N	22.9	2.54	0.8	36.0	34.2	0.95
$L = 122 \text{ cm}; \lambda = 55; f_y = 310 \text{ MPa}; A_s = 1.00 \text{ cm}^2$						
O	23.6	1.27	1.1	89.2	67.8	0.76
P	23.6	1.91	1.1	67.1	55.0	0.82
Q	19.9	2.54	1.2	50.2	42.2	0.84
$L = 274 \text{ cm}; \lambda = 125; f_y = 310 \text{ MPa}; A_s = 1.00 \text{ cm}^2$						
R	21.4	1.27	1.6	24.1	24.3	1.01
S	20.9	1.91	1.2	21.6	21.8	1.01
T	20.7	2.54	1.1	19.7	19.1	0.97

$R_m = 0.99$, the standard deviation is $\sigma_R = 0.06$ and the coefficient of variation is $V_R = \sigma_R/R_m = 0.06$. For columns under sustained loads, $R_m = 0.94$, $\sigma_R = 0.07$ and $V_R = 0.08$.

Figure 7 compares the measured and predicted variation of the moment $M = F(e_1 + W)$ with the load $N = F$ for the column C1 tested by Goyal and Jackson. The points represent the experimental results and the curve corresponds to the model. The variation of the first-order moment $M = Fe_1$, valid for short columns, is also presented in Figure 7.

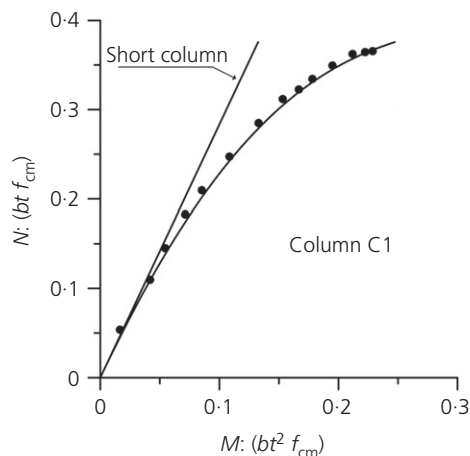


Figure 7. Load–moment curve for column C1

Columns tested by Tsao

Tsao (1991) tested six columns with square cross-sections and seven columns with L-shaped cross-sections, both types being subjected to biaxial bending. All columns have a length $L = 122 \text{ cm}$ and were subjected to short-term loads. For the columns with square cross-section, the slenderness ratios are $\lambda_x = \lambda_y = 55$. For columns with L-shaped cross-section, the slenderness ratios are $\lambda_x = 58$ and $\lambda_y = 43$.

Tables 3 and 4 present the results obtained for the columns tested by Tsao. For these 13 columns, $R_m = 1.00$, $\sigma_R = 0.09$ and $V_R = 0.09$.

Columns tested by Melo

Melo (2009) tested 21 columns of rectangular cross-section subjected to uniaxial bending. All columns have a steel area $A_s = 4.71 \text{ cm}^2$. The yield strength of reinforcement is $f_y = 595 \text{ MPa}$. Table 5 presents the results obtained for the columns tested by Melo. For these 21 columns, $R_m = 0.88$, $\sigma_R = 0.08$ and $V_R = 0.09$.

Columns tested by Kim and Yang

Kim and Yang (1995) tested 28 columns of square cross-section under uniaxial bending. The first-order eccentricity is $e_1 = 2.4 \text{ cm}$ for all columns. The columns have lengths $L = 24 \text{ cm}$, $L = 144 \text{ cm}$ and $L = 240 \text{ cm}$, corresponding to slenderness ratios $\lambda = 10$, $\lambda = 62$ and $\lambda = 104$, respectively. The yield strength of reinforcement is $f_y = 387 \text{ MPa}$.

Offprint provided courtesy of www.icevirtuallibrary.com
Author copy for personal use, not for distribution

Table 3. Columns with square cross-section tested by Tsao (1991)

Column	f_{cm} : MPa	f_y : MPa	e_x : cm	e_y : cm	$F_{u,exp}$: kN	$F_{u,teo}$: kN	$F_{u,teo}/F_{u,exp}$
C1	19.1	545	0.97	2.35	69.0	65.6	0.95
C2	18.6	545	1.80	1.80	57.0	62.7	1.10
C3	29.0	545	3.59	3.59	40.0	44.0	1.10
C4	25.5	421	1.80	1.80	84.8	71.2	0.84
C5	25.5	421	1.94	4.69	47.6	44.3	0.93
C6	25.5	421	0.97	2.35	83.2	73.2	0.88

Table 4. Columns with L-shaped cross-section tested by Tsao (1991)

Column	f_{cm} : MPa	f_y : MPa	e_x : cm	e_y : cm	$F_{u,exp}$: kN	$F_{u,teo}$: kN	$F_{u,teo}/F_{u,exp}$
B2	25.1	434	2.15	4.61	45.6	48.8	1.07
B3	26.8	434	2.69	2.69	57.0	55.3	0.97
B4	26.8	441	3.59	3.59	45.0	43.7	0.97
B5	29.3	441	0.90	0.90	128.2	120.5	0.94
B6	29.3	441	1.80	1.80	71.5	78.6	1.10
B7	29.2	441	1.55	2.01	71.5	81.5	1.14
B8	29.2	441	3.09	4.03	46.8	46.8	1.00

Table 5. Columns tested by Melo (2009)

Column	f_{cm} : MPa	e_i : cm	$F_{u,exp}$: kN	$F_{u,teo}$: kN	$F_{u,teo}/F_{u,exp}$
Columns with $L = 300$ cm; $\lambda = 87$					
6-3	39.6	0.6	652.0	599.8	0.92
12-3	39.6	1.2	535.0	460.1	0.86
15-3	35.8	1.5	446.5	375.1	0.84
18-3	39.7	1.8	460.5	345.4	0.75
24-3	39.7	2.4	241.0	255.5	1.06
30-3	33.9	3.0	254.8	188.6	0.74
40-3	33.9	4.0	170.2	149.8	0.88
50-3	37.6	5.0	155.0	136.4	0.88
60-3	37.6	6.0	131.0	121.8	0.93
Columns with $L = 250$ cm; $\lambda = 72$					
15-2.5	43.1	1.5	670.4	529.6	0.79
24-2.5	45.8	2.5	360.8	319.2	0.95
30-2.5	41.6	3.0	336.0	268.8	0.80
40-2.5	41.6	4.0	246.0	206.6	0.84
50-2.5	41.6	5.0	201.2	177.1	0.88
60-2.5	43.1	6.0	164.8	156.6	0.95
Columns with $L = 200$ cm; $\lambda = 58$					
15-2	38.5	1.5	662.0	582.6	0.88
24-2	45.8	2.5	456.0	446.9	0.98
30-2	37.2	3.0	317.0	317.0	1.00
40-2	37.2	4.0	294.4	244.4	0.83
50-2	37.2	5.0	232.0	206.5	0.89
60-2	38.5	6.0	198.4	180.5	0.91

Table 6 presents the results obtained for the columns tested by Kim and Yang. For these 28 columns, $R_m = 0.95$, $\sigma_R = 0.07$ and $V_R = 0.07$.

Columns tested by Kim and Lee

Kim and Lee (2000) tested 16 columns of rectangular cross-section under biaxial bending. All columns have a length

$L = 130$ cm. The mean compressive strength of concrete is $f_{cm} = 27$ MPa and the yield strength of reinforcement is $f_y = 436$ MPa.

Table 7 presents the results obtained for the columns tested by Kim and Lee. For these 16 columns, $R_m = 0.87$, $\sigma_R = 0.04$ and $V_R = 0.05$.

Offprint provided courtesy of www.icevirtuallibrary.com
Author copy for personal use, not for distribution

Table 6. Columns tested by Kim and Yang (1995)

Column	A_g : cm ²	L : cm	$F_{u,exp}$: kN	$F_{u,teo}$: kN	$F_{u,teo}/F_{u,exp}$
$f_{cm} = 25.5$ MPa					
L4-1	2.53	24	109.5	108.4	0.99
L4-2	2.53	24	109.3	108.4	0.99
L2-1	1.27	144	63.7	62.4	0.98
L2-2	1.27	144	65.7	62.4	0.95
L2-1	1.27	240	38.2	36.3	0.95
L2-2	1.27	240	35.0	36.3	1.04
L4-1	2.53	240	49.0	45.6	0.93
L4-2	2.53	240	47.0	45.6	0.97
$f_{cm} = 63.5$ MPa					
M2-1	1.27	24	179.0	164.7	0.92
M2-2	1.27	24	182.8	164.7	0.90
M4-1	2.53	24	207.7	182.8	0.88
M4-2	2.53	24	204.6	182.8	0.89
M2-1	1.27	144	102.8	98.7	0.96
M2-2	1.27	144	113.5	98.7	0.87
M2-1	1.27	240	45.2	48.4	1.07
M2-2	1.27	240	47.6	48.4	1.02
M4-1	2.53	240	59.6	63.2	1.06
M4-2	2.53	240	60.5	63.2	1.04
$f_{cm} = 86.2$ MPa					
H2-1	1.27	24	235.3	195.3	0.83
H2-2	1.27	24	240.4	195.3	0.81
H4-1	2.53	24	255.8	212.3	0.83
H4-2	2.53	24	257.7	212.3	0.82
H2-1	1.27	144	122.1	111.1	0.91
H2-2	1.27	144	123.7	111.1	0.90
H2-1	1.27	240	54.3	51.6	0.95
H2-2	1.27	240	54.9	51.6	0.94
H4-1	2.53	240	66.6	67.9	1.02
H4-2	2.53	240	64.7	67.9	1.05

Table 7. Columns tested by Kim and Lee (2000)

Column	e_x : cm	e_y : cm	$F_{u,exp}$: kN	$F_{u,teo}$: kN	$F_{u,teo}/F_{u,exp}$
Series RS ($\lambda_x = 22.5$; $\lambda_y = 45$)					
RS0-1	0	4.00	204	186	0.91
RS0-2	0	4.00	206	186	0.90
RS30-1	2.00	3.46	208	196	0.94
RS30-2	2.00	3.46	217	196	0.90
RS45-1	2.83	2.83	266	215	0.81
RS45-2	2.83	2.83	239	215	0.90
RS60-1	3.46	2.00	313	250	0.80
RS60-2	3.46	2.00	295	250	0.85
RS90-1	4.00	0.00	418	372	0.89
RS90-2	4.00	0.00	443	372	0.84
Series SS ($\lambda_x = 45$; $\lambda_y = 45$)					
SS0-1	0	4.00	119	106	0.89
SS0-2	0	4.00	126	106	0.84
SS30-1	2.00	3.46	112	93	0.83
SS30-2	2.00	3.46	104	93	0.89
SS45-1	2.83	2.83	103	91	0.88
SS45-2	2.83	2.83	106	91	0.86

Results for all columns

When considering all 124 columns, the ratio $R = F_{u,teo}/F_{u,exp}$ presented the mean value $R_m = 0.94$, standard deviation $\sigma_R = 0.08$ and coefficient of variation $V_R = 0.09$. Figure 8

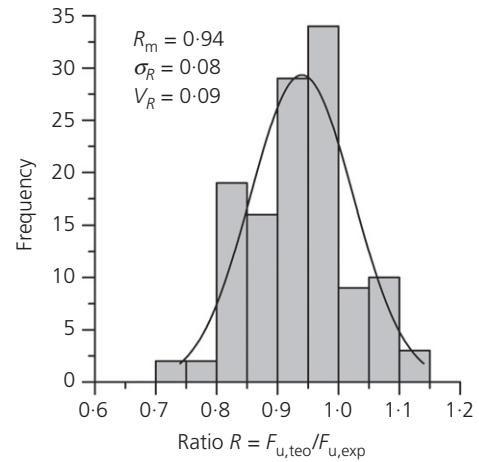


Figure 8. Histogram of $R = F_{u,teo}/F_{u,exp}$ for 124 columns

shows a histogram obtained for the 124 columns. It is observed that besides the good accuracy of the results, the model tends to be conservative, as desired.

Assuming a normal distribution, the fifth percentile is given by $R_1 = R_m - 1.645\sigma_R = 0.81$ and the 95th percentile is $R_2 = R_m + 1.645\sigma_R = 1.07$, so that 90% of the values of R should be in the range $[0.81 - 1.07]$. The range with 90% probability of occurrence is shown in Figure 9.

Considerations for the design of slender columns

The developed model can be used for the dimensioning of slender reinforced-concrete columns. In this case, it is necessary to make small changes in the stress-strain diagrams for materials in order to introduce partial safety factors. The design strengths for materials are given by $f_{yd} = f_{yk}/\gamma_s$ and $f_{cd} = f_{ck}/\gamma_c$, where f_{yk} is the characteristic yield strength of

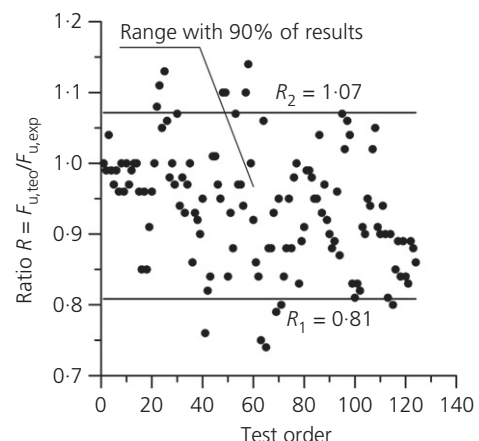


Figure 9. Range with 90% probability of occurrence

reinforcement and f_{ck} is the characteristic compressive strength of concrete. According to Eurocode 2 (BSI, 2004), the partial safety factors are $\gamma_s = 1.15$ and $\gamma_c = 1.5$ for persistent and transient design situations.

The stress–strain diagram of reinforcement is the same as shown in Figure 1, with f_y replaced by f_{yd} . Two parabola–rectangle diagrams must be used for concrete, as shown in Figure 10. The diagram **obc**, with maximum stress equal to $0.85f_{ck}$, is used to calculate the displacements of the column axis. The diagram **ode**, with maximum stress equal to $0.85f_{cd}$, is used to verify the failure by concrete crushing. Since $\sigma_c > 0.85f_{cd}$ is not allowed, it is possible to work with a single diagram **oadc**, as indicated in Figure 10. The strain ε_{co} corresponding to the stress $\sigma_c = 0.85f_{cd}$ is given by

$$15. \quad \varepsilon_{co} = \varepsilon_{c2} \left[1 - \left(1 - \frac{1}{\gamma_c} \right)^{1/n} \right]$$

Thus, the stress–strain relations for compressed concrete are given by

$$16. \quad \sigma_c = 0.85f_{ck} \left[1 - \left(1 - \frac{\varepsilon_c}{\varepsilon_{c2}} \right)^n \right], \quad \text{if } 0 \leq \varepsilon_c \leq \varepsilon_{co}$$

$$17. \quad \sigma_c = 0.85f_{cd}, \quad \text{if } \varepsilon_{co} \leq \varepsilon_c \leq \varepsilon_{cu2}$$

where the stress and strain are represented by their absolute values.

By employing Equation 9 to calculate the exponent n , the modulus of elasticity E_{cm} is replaced by $E_{cd} = E_{cm}/\gamma_{cE}$, where $\gamma_{cE} = 1.2$ according to Eurocode 2. The other aspects of the model remain unchanged.

The model can be easily implemented in existing software by simply changing the subroutine that calculates the stress in concrete. Equations 9, 15–17 are used, remembering that E_{cm} is replaced by $E_{cd} = E_{cm}/\gamma_{cE}$ in Equation 9.

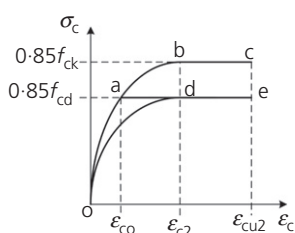


Figure 10. Parabola–rectangle diagrams for design

Conclusions

This paper presents a non-linear model for the analysis and design of slender reinforced-concrete columns subjected to uniaxial and biaxial bending. The model considers both material and geometric non-linearities, as well as creep effects. Structural analysis is performed using the finite-element method. The BFGS iterative method is used to solve the system of non-linear equations. Columns may have an arbitrary polygonal cross-section, including openings. The integrations necessary for the determination of sectional forces are performed using Green's theorem.

In the first part of this study, it was shown that the classical parabola–rectangle diagram, as presented in Eurocode 2 (BSI, 2004), cannot be used for non-linear analysis of slender columns because it provides incorrect and inconsistent values for the modulus of elasticity of concrete. This parabola–rectangle diagram is only recommended for the design of cross-sections. Eurocode 2 presents a stress–strain relation for non-linear structural analysis, but it is too complex to perform explicit integrations using Green's theorem.

To eliminate this difficulty, a new parabola–rectangle diagram is proposed to represent the stress–strain relationship for compressed concrete. Thus, the correct value of the tangent modulus of elasticity at the origin of the stress–strain diagram is obtained. This modified parabola–rectangle diagram can be used for non-linear analysis, unlike the original parabola–rectangle diagram of Eurocode 2. It has the advantage of being simpler than the stress–strain relation for non-linear structural analysis adopted by Eurocode 2. The use of the new parabola–rectangle diagram facilitates the integrations necessary to obtain the sectional forces through Green's theorem. By introducing the partial safety factor for concrete and modifying the strain value corresponding to the maximum stress, this diagram can be used for the design of slender columns.

The model was used to analyse 124 columns tested by other authors, with 20 columns subjected to sustained loads and 104 columns subjected to short-term loads. Tests include 95 columns subjected to uniaxial bending and 29 columns subjected to biaxial bending. The theoretical failure load $F_{u,teo}$ was compared with the experimental failure load $F_{u,exp}$ obtained in the tests. The ratio $R = F_{u,teo}/F_{u,exp}$ presented the mean value $R_m = 0.94$, the standard deviation $\sigma_R = 0.08$ and the coefficient of variation $V_R = 0.09$. It is concluded that, in addition to providing results with good accuracy, the model is conservative as desired.

REFERENCES

- ACI (American Concrete Institute) (2014) ACI 318-14: Building code requirements for structural concrete. American Concrete Institute, Farmington Hills, MI, USA.
Araújo JM (2014) *Curso de Concreto Armado*, 4th edn. Dunas, Rio Grande, Brazil (in Portuguese).

Offprint provided courtesy of www.icevirtuallibrary.com
Author copy for personal use, not for distribution

- Barros H, Silva VD and Ferreira C (2010) Second order effects in slender concrete columns-reformulation of the Eurocode 2 method based on nominal curvature. *Engineering Structures* **32(12)**: 3989–3993.
- Bonet JL, Romero ML, Miguel PF and Fernandez MA (2004) A fast stress integration algorithm for reinforced concrete sections with axial loads and biaxial bending. *Computers & Structures* **82(2–3)**: 213–225.
- Bonet JL, Romero ML, Fernandez MA and Miguel PF (2007) Design method for slender columns subjected to biaxial bending based on second-order eccentricity. *Magazine of Concrete Research* **59(1)**: 3–19, <https://doi.org/10.1680/mac.2007.59.1.3>.
- Bonet JL, Romero ML and Miguel PF (2011) Effective flexural stiffness of slender reinforced concrete columns under axial forces and biaxial bending. *Engineering Structures* **33(3)**: 881–893.
- Bouchaboub M and Samai ML (2013) Nonlinear analysis of slender high-strength R/C columns under combined biaxial bending and axial compression. *Engineering Structures* **48(3)**: 37–42.
- BSI (2004) BS EN 1992-1-1:2004+A1:2014: Eurocode 2: Design of concrete structures. General rules and rules for buildings. BSI, London, UK.
- CEB (Comite Euro-International du Beton) (1990) CEB-FIP Model Code 1990. CEB, Lausanne, Switzerland.
- fib (International Federation for Structural Concrete) (2010) *fib Model Code 2010*. International Federation for Structural Concrete, Lausanne, Switzerland.
- Goyal Brij B and Jackson N (1971) Slender concrete columns under sustained load. *Journal of the Structural Division, ASCE* **97(11)**: 2729–2750.
- Kim JK and Lee SS (2000) The behavior of reinforced concrete columns subjected to axial force and biaxial bending. *Engineering Structures* **22(11)**: 1518–1528.
- Kim JK and Yang JK (1995) Buckling behaviour of slender high-strength concrete columns. *Engineering Structures* **17(1)**: 39–51.
- Kwak HG and Kim JK (2004) Ultimate resisting capacity of slender RC columns. *Computers & Structures* **82(11–12)**: 901–915.
- Lou T, Lopes SMR and Lopes AV (2015) FE analysis of short- and long-term behavior of simply supported slender prestressed concrete columns under eccentric end axial causing uniaxial bending. *Engineering Structures* **85(4)**: 52–62.
- Melo CEL (2009) *Análise experimental e numérica de pilares birrotulados de concreto armado submetidos a flexo-compressão normal*. DEng thesis, Department of Civil and Environmental Engineering, UnB, Brasília, Brazil (in Portuguese).
- Narayanan RS and Beeby AW (2005) *Designer's Guide to EN1992-1-1 and EN1992-1-2 Eurocode 2: Design of Concrete Structures*, 1st edn. Thomas Telford, London, UK.
- Pires SL and Silva MCAT (2014) A numerical procedure for reinforced concrete columns with a focus on stability analysis. *Computers and Concrete* **14(6)**: 657–674.
- Tsao WH (1991) *Behavior of Square and L-shaped Slender Reinforced Concrete Columns under Combined Biaxial Bending and Axial Compression*. Doctoral thesis, New Jersey Institute of Technology, Newark, NJ, USA.
- Zienkiewicz OC and Taylor RL (2000) *The Finite Element Method*, 5th edn. Butterworth-Heinemann, Oxford, UK.

How can you contribute?

To discuss this paper, please submit up to 500 words to the editor at journals@ice.org.uk. Your contribution will be forwarded to the author(s) for a reply and, if considered appropriate by the editorial board, it will be published as a discussion in a future issue of the journal.